Heat Transfer and Pressure Drop in Heat Exchangers

DANIEL A. DONOHUE

The Lummus Company, New York 11, N. Y.

A correlation of the coefficient of heat transfer in unbaffled shells has been developed from the published experimental data which differs considerably from that presently used. For any particular baffled shell the coefficient of heat transfer is expressed by the relation

$$\frac{hD}{k} = C\left(\frac{DG_e}{\mu}\right)^{0.6}\left(\frac{c\mu}{k}\right)^{0.33}\left(\frac{\mu}{\mu_w}\right)^{0.14}$$

in which G_e is the geometric mean of the mass velocities across the tube bundle and through the baffle opening. While G_e takes account of variations in baffle spacing and size of baffle opening, C accounts for all other shell-side structural characteristics—namely, arrangement of tubes within the shell and leakage areas. C has numerical values which, from the experimental data available, appear to be fairly constant for a given type of exchanger. Pressure drop tests show that only partial flow penetration of the tube bundle occurs. The effect of this partial flow penetration on coefficient of heat transfer and on friction factor is considered. Interdependency of the coefficient of heat transfer and friction factor is noted. Higher coefficients of heat transfer were obtained with disk-and-doughnut baffles than with segmental baffles for equal values of fluid flow rate and pressure drop in all units tested.

ALTHOUGH shell-and-tube heat exchangers in their present form have been used in this country for approximately 30 years, published information about heat transfer coefficient and pressure drop on the shell side is conflicting and until recently has been scarce. The purpose of this paper is to study the available experimental data of the different investigators and to present the underlying pattern which is revealed. Factors influencing heat transfer coefficient and pressure drop, in unbaffled and baffled shells, are identified and evaluated. In many of the experimental tests referred to in this paper, the technique employed was to vary only one condition while all others remained constant, thus permitting the effect of that variable to be observed.

SHELL-AND-TUBE HEAT EXCHANGER

A view of a commonly used heat exchanger is shown in Figure 1. This exchanger has a single-pass shell and two-pass tubes and is of the floating-head, removable-tube-bundle–type of construction. The fluid flowing outside the tubes enters the unit through the shell inlet nozzle and after being directed back and forth across the tubes by means of segmental baffles leaves through the shell outlet nozzle. The other fluid enters the unit through the channel inlet nozzle and flows through the first tube pass into the floating-head cover, where after reversing its direction, it flows through the second tube pass into the channel which it leaves through the channel outlet nozzle. To withdraw the tube bundle for cleaning, it is pulled through the channel end of the shell after both the floating-head cover and the backing ring have been unbolted and removed from the floating tube sheet. The principal path of flow around the baffling is shown in Figure 2 by the line labeled as main stream. Figure 2 also indicates that part of the flow leaks through clearance areas B-S, located between the periphery of the baffle and the inside circumference of the shell; and T-B, between tube and tube hole in the baffle. A view of the fluid flowing across the tube bundle in Figure 3 shows that not all of the flow penetrates (P_1) the tube bundle; some by-passes (B), flowing into the dead area between the tube bundle and the inside circumference of the shell. If there were no leakage or by-passing areas, an idealized flow path in a segmentally baffled shell could be represented as shown in Figures 4A and B by the broken lines. Segmental baffles are formed by cutting out thin, circular, metal plates to an outside diameter slightly less than the inside diameter of the shell. A segment is cut out of the baffle along a horizontal chord as shown in Figure 5 to form a segmental opening the size of which may vary from approximately

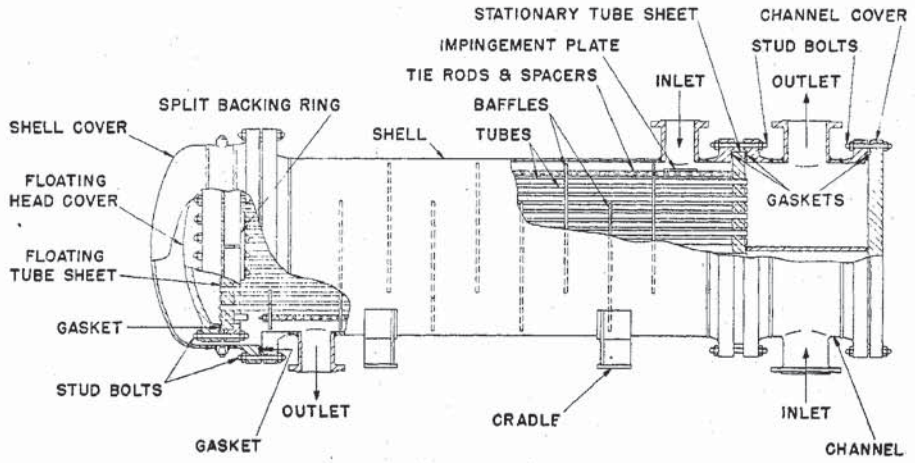

Figure 1. Floating-Head, Removable-Tube-Bundle–Type Heat Exchanger

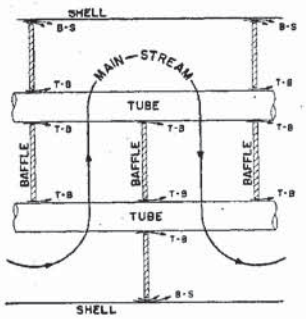

Figure 2. Cross-Sectional View of Exchanger with Segmental Baffles

Taken at C-C of Figure 5 along tube length. Baffle cutout 1.21 inches beyond center line

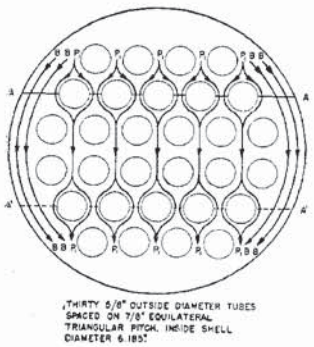

Figure 3. Flow across Tube Bundle of Heat Exchanger with Segmental Baffles

P_1, flow paths penetrating tube bundle; B, flow paths by-passing tube bundle; AA, baffle cut; $A'A'$, baffle cut of successive baffle

15 to 45% of the shell area. Holes in the baffle through which the tubes pass are drilled slightly larger than the tube diameter. Clearance areas B-S and T-B are usually kept to a minimum consistent with manufacturing practice.

In unbaffled shells fluid enters the unit through the shell inlet nozzle and leaves through the outlet nozzle after flowing parallel to the tube length located between nozzles.

Another form of baffling is the disk-and-doughnut type. The disk baffle has an annular flow area between the periphery of the baffle and the inside circumference of the shell; and the doughnut baffle has a circular opening for flow at the center of the baffle. The disk and the doughnut baffles are placed alternately on equal spacing, and fluid flows from the center of a doughnut baffle in a radial direction to the periphery of the next disk baffle, thence back radially to the center of the next doughnut baffle.

It would be desirable to fill the enclosing, heat-exchanger shell with tubes uniformly spaced; however, in industrial heat exchangers structural requirements prevent it. There are two kinds of areas which must be left unoccupied by tubes; (*a*) the annular area between the inside circumference of the shell and the outer most tubes, in Figure 1 the size of this area is governed by the width of the gasket at the bolted joint of the floating-head cover, and (*b*) lanes in the tube layout which are necessary to leave room for partition plates in the channel or floating head. It is seen, therefore, that there are several open paths in the exchanger among which the fluid will simultaneously distribute itself in accordance with the principle that the pressure drops through all paths will be equal. Fluid flow is sensitive to seemingly small variations in shell-side structure which affect these paths.

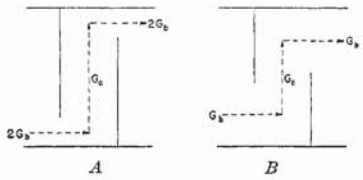

Figure 4. Effect of Size of Baffle Opening

COEFFICIENT OF HEAT TRANSFER

The relation involving heat transfer coefficient for turbulent flow is

$$\frac{hD}{k} = C\left(\frac{DG}{\mu}\right)^{n}\left(\frac{c\mu}{k}\right)^{0.33}\left(\frac{\mu}{\mu_w}\right)^{0.14} \quad (1)$$

in which n equals 0.8 when the flow takes place inside a tube and 0.6 when outside the tube. For flow inside circular cross sections the value of G, mass velocity, is simply equal to the flow rate, w, divided by the cross-sectional area. However, for flow outside tubes, the structural nature of the passage presents several different areas for simultaneous flow among which the fluid distributes itself. The evaluation of this complex flow pattern presents difficulties. Practical and simple methods of evaluating G will be developed presently.

The first step in obtaining the shell-side coefficient of heat transfer from the experimental test data was to calculate the over-all coefficient of heat transfer for the unit which equals the rate of heat transfer, B.t.u. per hour, divided by the product of the external tube surface, square feet, and the logarithmic mean temperature difference, ° F. Since, from the familiar concept of component coefficients, this over-all coefficient of heat transfer is composed of the five individual coefficients of shell fluid, fouling outside tubes, tube metal, fouling inside tube, and tube fluid it becomes necessary to evaluate the sum of the above items, the second through the fifth, and subtract the reciprocal of this value from the reciprocal of the over-all coefficient of heat transfer which yields the reciprocal of the shell-side coefficient of heat transfer.

For the majority of the experimental data (*6, 7, 13, 14*) the reciprocal of the combined coefficient of heat transfer of items two through five was evaluated by the well-known method of Wilson (*18*). In this method the reciprocal of the 0.6 power of the rate of shell fluid flow is plotted as abscissa, and the reciprocal of over-all coefficient of heat transfer, as ordinate. For a series of tests on a unit in which rate of flow of shell fluid is the only variable, a straight line results which, when extrapolated to zero rate of flow, intercepts the ordinate at a value which is taken as equal to the reciprocal of the sum of the coefficients of heat transfer for items two through five. For the remainder of the experimental data (*8, 17*), which involved viscous oils, items two, three, and four were considered to be negligible and item five, coefficient of heat transfer inside the tube, was calculated from the relation of Sieder and Tate (*16*).

UNBAFFLED SHELLS

In an unbaffled shell fluid flows parallel to the tube length. In the absence of any experimental evidence it has been felt that the unbaffled shell could be likened to a tube. For turbulent flow inside tubes the equation of Sieder and Tate (*16*) is

$$\frac{hD}{k} = 0.027\left(\frac{D_i G_t}{\mu}\right)^{0.8}\left(\frac{c\mu}{k}\right)^{0.33}\left(\frac{\mu}{\mu_w}\right)^{0.14} \quad (2)$$

where D_i = inside tube diameter, ft. G_t = mass velocity inside tube = total flow (lb./hr.)/cross-sectional area of tube, sq. ft. Substitution of D_e for D_i and G_u for G_t in Equation 2 does not yield a relation valid for the experimental data on unbaffled shells where D_e = equivalent diameter of cross-sectional area, ft. and G_u = mass velocity parallel to tubes = total flow (lb./hr.)/(cross-sectional area of shell − cross-sectional area of tubes).

Tests on unbaffled shells have been reported by Short (*14*) who tested six units in which water was cooled, and by Heinrich and Stückle (*8*) who tested one unit in which oil was cooled. The results of these investigators are plotted in Figure 6 which reveals a series of parallel lines, one for each unit. The lines of Figure 6 represent an equation of the general form

$$\frac{hD}{k} = C\left(\frac{DG_u}{\mu}\right)^{0.6}\left(\frac{c\mu}{k}\right)^{0.33} \quad (3)$$

where C = numerical constant varying with each unit
D = outside tube diameter

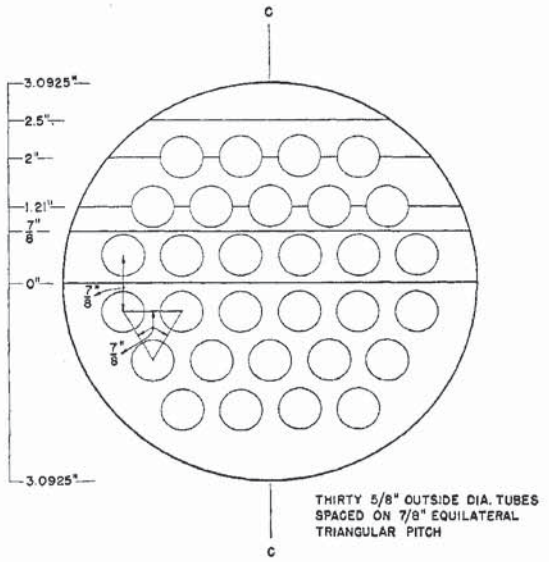

Figure 5. Various Sizes of Baffle Cutout, Unit 9-S

TABLE I. UNBAFFLED SHELLS

Correlated by equation $\frac{hD}{k} = 0.128\,(D_e')^{0.6}\left(\frac{DG_u}{\mu}\right)^{0.6}\left(\frac{c\mu}{k}\right)^{0.33}$

Experimenter	Short	Short	Short	Short	Short	Short	Heinrich and Stückle
Unit	1-S	2-S	3-S	5-S	7-S	9-S	Heinrich and Stückle
Shell, inside diameter, in.	6.06	6.06	6.06	6.06	6.06	6.06	10.82[a]
Tube, outside diameter, in.	3/8	3/8	1/2	1/2	1/2	5/8	0.449
Tube pitch (equilateral triangle), in.	1/2	11/16	19/32	25/32	13/32	7/8	.....
Number tubes	98	52	66	40	20	30	294
Flow area, sq. ft.	0.1212	0.156	0.1062	0.142	0.169	0.1326	0.0528
Equivalent diameter of cross-sectional area, in.	0.52	1.12	0.5	1.0	1.94	0.98	0.355
Shell-side fluid	Water	Water	Water	Water	Water	Water	Oil
Viscosity at 150° F., centipoises	0.432	0.432	0.432	0.432	0.432	0.432	10.6
Heated or cooled	C	C	C	C	C	C	C
Range of Reynolds number in Equation 3	1,310–9,160	951–6,640	1,580–12,500	868–10,200	940–8,750	1,420–13,270	232–1,072
Value of C in Equation 3	0.102	0.12	0.095	0.144	0.16	0.138	0.073

[a] Six pass shell divided into equal sectors.

The effect of viscosity gradient on the coefficient of heat transfer could not be evaluated because all tests were cooling operations in which the ratio of μ to μ_w varied only slightly. Two important facts may be noted from Equation 3: First, the exponent of the Reynolds number is 0.6 and not 0.8 as in Equation 2, and second, the value of C for the topmost line of Figure 7 is 2.25 times that for the lowest line.

In seeking an explanation of the variation of values of C in Equation 3 it was found that for this case of simple flow the only pertinent variable was the arrangement of the tubes within the shell. When values of C for each unit were plotted against the equivalent diameter they were found to vary with the 0.6 power of the equivalent diameter conforming to the relation

$$C = 0.128(D_e')^{0.6} \tag{4A}$$

C, as defined in Equation 4A, was substituted in Equation 3 to yield the relation

$$\frac{hD}{k} = 0.128(D_e')^{0.6}\left(\frac{DG_u}{\mu}\right)^{0.6}\left(\frac{c\mu}{k}\right)^{0.33} \tag{5}$$

All test points were correlated in Figure 7 with an average deviation of ±12% from Equation 5 which is represented by the solid line. Table I lists the range of variables encountered in the tests to which this correlation applies. It appears that the variation of heat transfer coefficient with equivalent diameter is a result of the effect of tube arrangement in controlling the pattern of flow. The two areas open to fluid flow are the annular area surrounding the tube bundle which is bounded by the inside shell circumference and by the outermost tubes, and the free area inside the tube bundle itself. These two flow areas present two parallel areas to flow and since the pressure drop through each area must be the same, the fraction of fluid flowing through each area must adjust itself to produce this condition. Increasing the tube pitch while maintaining essentially the same annular area reduces the frictional resistance of the tube bundle, thereby permitting a higher fraction of the flow to penetrate the tube bundle and producing higher heat transfer coefficient.

SEGMENTAL BAFFLES

There are four structural factors which influence G and consequently h in segmentally baffled shells. These are: baffle spacing, size of baffle opening, leakage areas, and tube arrangement. The effect of each of these factors was explored by varying only the factor under consideration while all other conditions were maintained constant.

BAFFLE SPACING. The experimental values obtained by Short (*14*) with his unit 9-S using 19, 15, 11, 7, and 3 baffles are plotted in Figure 8 which reveals a series of parallel lines expressed by an equation of the form

$$\frac{hD}{k} = C\left(\frac{DG_c}{\mu}\right)^{0.6}\left(\frac{c\mu}{k}\right)^{0.33} \tag{6}$$

Values of G_c, crossflow mass velocity, were taken along the shell diameter perpendicular to flow. The parallel lines of Figure 8 show that the value of C increases with increase in baffle spacing at constant crossflow mass velocity—for example, the line for the 3-baffle unit has a value of C 1.8 times that of the line for the 19-baffle unit. The experimental test figures of Bowman (*1*) for an 8-inch diameter, industrial exchanger are plotted in Figure 9 using crossflow mass velocity along the shell diameter perpendicular to flow. Figure 9 shows a series of parallel lines of the form expressed by Equation 6. In like manner these lines have C values which increase with baffle spacing; the line for 4-inch baffle spac-

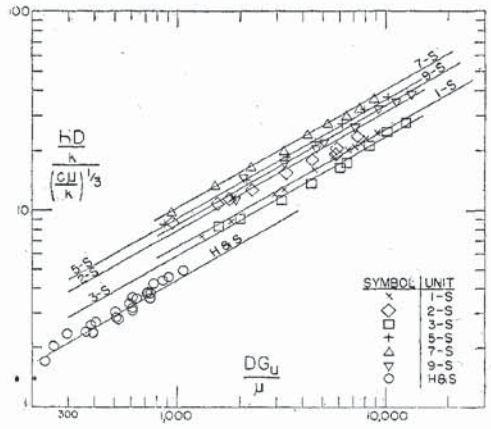

Figure 6. Heat Transfer Coefficient, h, Unbaffled Shells

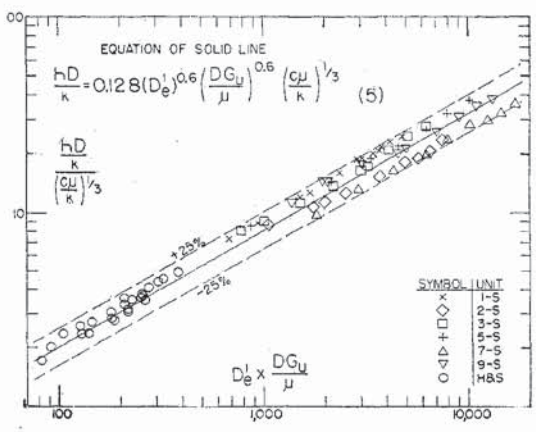

Figure 7. Heat Transfer Coefficient, h, Unbaffled Shells

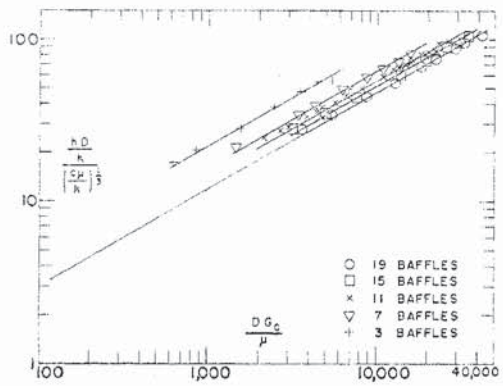

Figure 8. Various Segmental Baffle Spacings, Unit 9-S

ing has a C value 1.72 times that of the line for $^{29}/_{32}$-inch baffle spacing at the same value of crossflow mass velocity.

Figures 8 and 9, each of which applies to a given unit wherein the only variable is baffle spacing, demonstrate that the use of G_c in Equation 6 does not satisfactorily correlate the data, instead coefficients of heat transfer increase with increase in baffle spacing. The reason for this will become apparent from the following analysis:

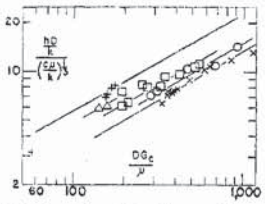

Figure 9. Various Segmental Baffle Spacings, Unit 8-B

× = 29/32-inch B.P.; ○ = 1.36-inch B.P.; □ = 1 13/16-inch B.P.; △ = 2 41/64-inch B.P.; + = 4-inch B.P.

Figures 10A and B represent an analysis of the path for fluid flow in a segmentally baffled unit. The baffle spacing in Figure 10B is three times that in Figure 10A but all other dimensions, size of baffle opening, number and diameter of tubes, and tube spacing are the same. When three times as much fluid flows through Figure 10B as through Figure 10A the crossflow velocity, G_c, will be the same in each unit. However, since the baffle openings in each exchanger are equal the velocity through the baffle opening of Figure 10B, designated as $3G_b$, is three times the velocity through the baffle opening of Figure 10A, G_b. With equal crossflow mass velocities in each exchanger and a velocity through the baffle opening three times as great in Figure 10B as in Figure 10A it would seem that the exchanger of Figure 10B should have a higher heat transfer coefficient than the exchanger shown in Figure 10A when the correlation is based on G_c. This has been the evidence of Figures 8 and 9.

It was found that experimental test figures for any heat exchanger in which the only variable was baffle spacing could be correlated by use of a weighted velocity which took into account velocities at two separate locations—across the tube bank and through the baffle hole. The area on which the weighted velocity is based is the geometric mean of the crossflow and the baffle-hole areas.

$$S_e = \text{weighted flow area} = \sqrt{\text{crossflow area} \times \text{baffle-hole area}} \quad (7)$$

The weighted mass velocity is

$$G_e = w/S_e = (G_c G_b)^{0.5} \quad (8)$$

Variations in baffle spacing may be correlated by use of the following relation

$$\frac{hD}{k} = C\left(\frac{DG_e}{\mu}\right)^{0.6}\left(\frac{c\mu}{k}\right)^{0.33} \quad (9)$$

The data for unit 9-S which were shown in Figure 8 plotted against Equation 6 are now shown in Figure 11 plotted against Equation 9. The value of C in Equation 9 for the solid line of Figure 11 is 0.2.

The magnitude of the effect which baffle spacing can exert on the value of C in Equation 9 may be found by substituting values of the ratio of the crossflow area to the baffle-opening area for the units listed in Tables II, III, and IV in this equation. The ratio of crossflow area to baffle-opening area which ranges from 0.337 to 9 will cause C to range from relative values of 1 to 2.68.

Size of Baffle Opening. In order to observe the effect of variation of size of baffle opening, Short (*13*) tested unit 9-S which had the inside of its shell bored to a uniform diameter. A cross-sectional view of this unit is shown in Figure 5 with different sizes of baffle cutout located 2.5 inches, 2 inches, 1.21 inches, and 0 inch above the horizontal shell diameter. Other units in which the only variable was size of baffle cutout were units 9-T and 10-T of Tinker (*17*) which are described in Table IV. The data of Short for unit 9-S are plotted by use of Equation 6 in Figures 12 and 13 and those of Tinker for units 9-T and 10-T by the same method in Figure 14. These figures show that the smaller the baffle opening the higher will be the value of C in Equation 6 for similar values of Reynolds number based on velocity across the tube bundle. This will be readily understood by reference to Figures 4A and B which show two units similar in every respect except that Figure 4B has a baffle opening twice that of Figure 4A. As shown, the rate of flow, pounds per hour, is the same in each unit. Under this condition the crossflow mass velocity, G_c, in each unit is equal, but the mass velocity through the baffle opening in Figure 4A designated as $2G_b$, is twice that in Figure 4B, G_b. Therefore, with equal crossflow velocities and a velocity through the baffle opening in Figure 4A twice that in Figure 4B, it would be expected that a higher heat transfer coefficient (or C value) would be obtained with Figure 4A than with Figure 4B.

Table V has been compiled to determine whether or not Equation 9, employing the geometric mean mass velocity G_e, can be used to correlate satisfactorily the data for a unit in which the only variable is the size of baffle opening. For the purpose of effecting a comparison, values of heat transfer coefficient were calculated for the units listed in Table V and these values were compared with those obtained experimentally which were plotted in Figures 12 to 14. Reference to the last line of Table V shows that this method is adequate except for unit 9-S (1a). This unit had its baffle cutout located 2.5 inches above the horizontal diameter, and examination of Figure 5 reveals that observed values of heat transfer coefficient were low because the baffle cutout was not long enough to direct the flow across the entire width of the tube bundle, thereby rendering some of the tubes ineffective for heat transfer. Therefore, it appears that the smallest size baffle cutout should be approximately 15% while the largest size, as dictated by structural considerations, is 45% of the shell cross-sectional area.

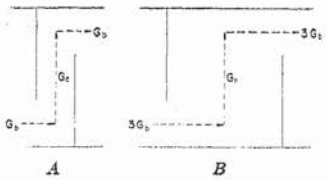

Figure 10. Effect of Baffle Spacing

The effect which variations in size of baffle opening can exert on values of C in Equation 9 is not nearly so great as that possible with variation of baffle spacing, for the

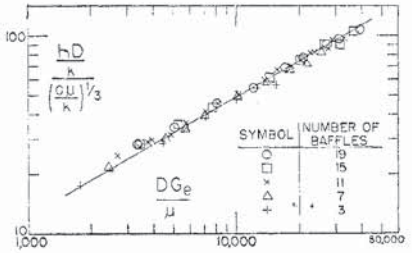

Figure 11. Various Segmental Baffle Spacings, Unit 9-S

TABLE II. SEGMENTAL BAFFLES, SHORT'S (*14*) UNBORED SHELLS

Correlated by equation $\frac{hD}{k} = 0.19\,(D_e')^{0.6}\left(\frac{DG_e}{\mu}\right)^{0.6}\left(\frac{c\mu}{k}\right)^{0.33}$

Unit	1-S	2-S	3-S	4-S	5-S	6-S	7-S	8-S	9-S		10-S	
Shell, inside diameter, in.	6.06	6.06	6.06	6.06	6.06	6.06	6.06	6.06	6.06		6.06	
Tube, outside diameter, in.	3/8	3/8	1/2	1/2	1/2	1/2	1/2	5/8	5/8		5/8	
Tube pitch (equilateral triangle), in.	1/2	11/16	19/32	11/16	25/32	1	1 3/32	3/4	7/8		1 1/16	
Number tubes	98	52	66	48	40	30	20	40	30		20	
Diameter of baffle hole-tube diameter, in.	1/64	1/64	1/64	1/64	1/64	1/64	1/64	1/64	1/64		1/64	
Inside shell diameter-baffle diameter, in.	Unbored shell	Unbored shell	Unbored shell	Unbored shell	Unbored shell	Unbored shell	Unbored shell	Unbored shell	Unbored shell		Unbored shell	
Crossflow area, sq. ft.	0.0313-0.287	0.0495-0.456	0.0253-0.233	0.0333-0.285	0.0415-0.382	0.0495-0.456	0.0574-0.528	0.0273-0.252	0.0374-0.345		0.0474-0.437	
Baffle cutout area, sq. ft.	0.0417	0.052	0.0386	0.0461	0.0468	0.0507	0.0562	0.0387	0.0437		0.0528	
Equivalent diameter of cross-sectional area, in.	0.52	1.12	0.5	0.8	1.0	1.35	1.94	0.66	0.98		1.52	
Shell-side fluid	Water	Water	Water	Water	Water	Water	Water	Water	Water	Oil B	Water	Oil A Oil B
Viscosity at 150° F., centipoises	0.432	0.432	0.432	0.432	0.432	0.432	0.432	0.432	0.432	18.6	0.432	7.7 18.6
Heated or cooled	C	C	C	C	C	C	C	C	C		C	
Range of Reynolds number in Equation 6	496-30,800	322-22,800	490-40,200	455-41,300	434-31,300	413-30,700	328-26,600	737-50,700	57.8-41,700		50.3-39,300	
Value of C in Equation 9	0.133	0.191	0.133	0.184	0.191	0.215	0.242	0.163	0.2		0.237	
Effective $\% h = 100\ C/0.33$	40.3	57.9	40.3	55.8	58	65.2	73.3	49.4	60.6		71.9	
Effective $\% \Delta p_e = 100\ f$ (observed)$/f$ (calculated for full flow penetration)	11.3	61	20	22.5	49	81	100	26	85		100	

simple reason that size of baffle opening can range only from 15 to 45% of the cross-sectional area of the shell which corresponds to a relative range of C from 1 to 1.39.

LEAKAGE AREAS. Experiments with shells bored to a uniform diameter wherein the clearance between baffles and shell was the only variable were reported by Short (*13*) and also by Tinker (*17*); the variables of these tests are listed in Table IV. In order to show the effect of variation of leakage area on heat transfer coefficient, the experimental data of Short (*13*) for those of his units which had the minimum size baffle opening with various baffle spacings and various clearances were plotted by use of Equation 9 in Figure 15, and the magnitude of decrease in heat-transfer coefficient with increase in leakage area is shown. In Figure 16 Short's (*13*) data for all other baffle openings with various baffle spacings and various clearances are plotted and it is seen that despite numerous structural variations in baffle spacing, clearances, and size of baffle opening in these units the maximum deviations from the correlating line are approximately ±15%.

Two units tested by Tinker (*17*), 2-T and 3-T, in which the only difference was the clearance area show a decrease of 19%

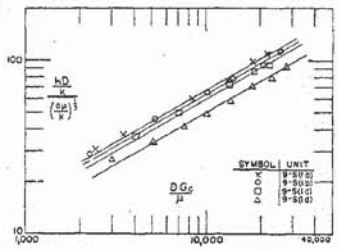

Figure 12. Various Sizes of Segmental Baffle Cutout

Short's tests; 11 baffles each unit

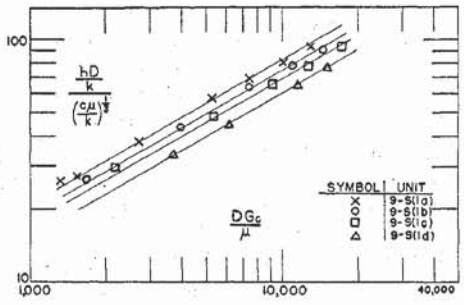

Figure 13. Various Sizes of Segmental Baffles Cutout

Short's tests; 19 baffles each unit

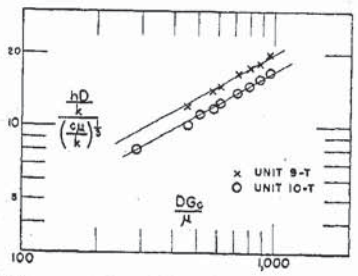

Figure 14. Various Sizes of Segmental Baffle Cutout

Tinker's tests

TABLE III. SEGMENTAL BAFFLES, BOWMAN'S (*1*) UNBORED SHELLS

Correlated by equation $\frac{hD}{k} = 0.22\left(\frac{DG_e}{\mu}\right)^{0.6}\left(\frac{c\mu}{k}\right)^{0.33}\left(\frac{\mu}{\mu_w}\right)^{0.14}$

Unit	6-B	8-B	10-B	12-B	16-B	24-B
Shell, inside diameter, in.	6	8	10	12	15¼	23¼
Tube, outside diameter, in.	5/8	5/8	5/8	5/8	5/8	1
Tube pitch (equilateral triangle), in.	23/22	13/16	13/16	13/16	13/16	1-3/16
Number tubes	28	44	76	122	199	250
Inner shell diameter–baffle diameter, in.	Unbored shell	Unbored shell	Unbored shell	Unbored shell	Unbored shell	Unbored shell
Crossflow area, sq. ft.	0.014	0.0208-0.092	0.0535	0.146	0.404	0.1627-0.252
Baffle cutout area, sq.ft.	0.0169	0.01306	0.0611	0.0697	0.1438	0.216
Equivalent diameter of cross-sectional area, in.	0.95	1.13	1.23	1.09	1.11	1.07
Shell-side fluid	Oil	Oil	Oil	Oil	Oil	Oils
Viscosity at 150° F., centipoises	18.2	12.4	31.4	18.2	32.6	12.4, 51.2
Heated or cooled	C	C	C	C	C	C
Range of Reynolds number in Equation 6	103-396	57-1,140	161-272	38-102	38-77	78-1,583
Value of C in Equation 11A	0.31	0.21	0.23	0.26	0.20	0.20

TABLE IV. SEGMENTAL

Correlated by equation $\frac{hD}{k}$ =

Experimenter	Short	Short	Short	Short	Short	Short	Short	Short	Short	Short
Unit	9-S(1a)	9-S(1b)	9-S(1c)	9-S(1d)	9-S(2a)	9-S(2c)	9-S(3a)	9-S(4a)	9-S(4c)	9-S(4d)
Shell, inside diameter, in.	6.185	6.185	6.185	6.185	6.185	6.185	6.185	6.185	6.185	6.185
Tube, outside diameter, in.	5/8	5/8	5/8	5/8	5/8	5/8	5/8	5/8	5/8	5/8
Tube pitch (equilateral triangle), in.	7/8	7/8	7/8	7/8	7/8	7/8	7/8	7/8	7/8	7/8
Number tubes	30	30	30	30	30	30	30	30	30	30
Diameter of baffle hole-tube diameter, in.	0.005	0.005	0.005	0.005	0.005	0.005	0.005	0.005	0.005	0.005
Inside shell diameter–baffle diameter, in.	0.06	0.06	0.06	0.06	0.125	0.125	0.185	0.255	0.255	0.255
Crossflow area, sq. ft.	0.0394–0.362	0.0394–0.0718	0.0394–0.362	0.0394–0.0718	0.0394–0.0718	0.0394–0.0718	0.0394–0.0718	0.0394–0.0718	0.0394	0.0394
Baffle cutout area, sq. ft.	0.01013[a]	0.0207	0.0403	0.0726	0.01013[a]	0.0403	0.01013[a]	0.01013[a]	0.0403	0.0726
Equivalent diameter of cross-sectional area, in.	0.98	0.98	0.98	0.98	0.98	0.98	0.98	0.98	0.98	0.98
Shell-side fluid	Water	Water	Water	Water	Water	Water	Water	Water	Water	Water
Viscosity at 150° F., centipoises	0.432	0.432	0.432	0.432	0.432	0.432	0.432	0.432	0.432	0.432
Heated or cooled	C	C	C	C	C	C	C	C	C	C
Range of Reynolds number in Equation 12	2,440–44,500	3,100–35,100	2,250–28,500	2,180–21,100	4,460–37,900	2,900–31,800	4,290–43,000	3,920–49,800	3,260–23,400	3,330–19,200
Value of C in Equation 12	0.18	0.215	0.235	0.235	0.17	0.232	0.165	0.147	0.21	0.21
Effective % h = 100 C/0.33	....	65.2	71.3	71.3	....	70.3	....	....	63.6	63.6
Effective % Δp_e = 100 f (observed)/f (calculated for full flow penetration)	....	...	....	...	....	...	....	....	...	...
% flow penetration from effective % h	....	49	56.9	56.9	....	55.5	....	....	47.1	47.1
% flow penetration from effective % Δp_e	....	...	...	...	....	...	....	....	...	...
% h/% Δp_e	....	...	...	...	....	...	....	....	...	...

[a] Baffle cutout not long enough to direct flow across entire width of tube bundle.

in heat transfer coefficient as a consequence of the increase in leakage area.

TUBE ARRANGEMENT. It has been noted in the analysis of unbaffled shells, in which flow was parallel to the tubes, that the flow pattern and consequently the heat transfer coefficient were influenced by the arrangement of the tubes within the shell. Similar effects were observed with the units tested by Short (*14*) listed in Table II. The experimental data for these units were correlated by use of Equation 9 in which the value of C differed for each unit. When C was plotted against D_e' for each unit the relation,

$$C = 0.19\,(D_e')^{0.6} \tag{4B}$$

was found to hold. Combination of Equations 9 and 4*B* produced the relation

$$\frac{hD}{k} = 0.19(D_e')^{0.6}\left(\frac{DG_e}{\mu}\right)^{0.6}\left(\frac{c\mu}{k}\right)^{0.33} \tag{10}$$

Figure 17 shows the 462 experimental test figures of Short (*14*) for 10 different units each having from three to five different baffle spacings, plotted against the solid line representing Equation 10. Two broken, boundary lines are shown to indicate points within ±25% of this line; most of the points fall within these limits, the average deviation of the test points from Equation 10 being ±9%.

While the units listed in Table II exhibited considerable variation in values of C in Equation 9, those industrial heat exchangers tested by Bowman (*1*) which are listed in Table III, and by Tinker (*17*) which are listed in Table IV gave evidence of more constant values for C. The experimental tests of Bowman (*1*) which are plotted in Figure 18 were correlated by the equation

$$\frac{hD}{k} = 0.22\left(\frac{DG_e}{\mu}\right)^{0.6}\left(\frac{c\mu}{k}\right)^{0.33}\left(\frac{\mu}{\mu_w}\right)^{0.14} \tag{11A}$$

In Figure 19 the data for the exchangers tested by Tinker (*17*) are correlated by the equation

$$\frac{hD}{k} = 0.25\left(\frac{DG_e}{\mu}\right)^{0.6}\left(\frac{c\mu}{k}\right)^{0.33}\left(\frac{\mu}{\mu_w}\right)^{0.14} \tag{11B}$$

The comparative constancy in values of C for the industrial units appears to result from the comparative constancy of tube arrangement within all shells which tended to stabilize the amount of flow penetrating the tube bundles. For these industrial units, use of the equivalent diameter, employed in Equation 10 to correlate Short's data, was unnecessary.

Viscosity Gradient. The most extensive data for heating and cooling operations in the same exchanger using oils of widely different viscosities are those of Gardner and Siller (*6*, *7*). Their experimental data for 990 Oil when correlated by use of Equation 9 showed heat transfer coefficients approximately 80% higher for heating than for cooling. These and all other data were correlated by use of the viscosity-gradient term $(\mu/\mu_w)^{0.14}$ which when incorporated into Equation 9 yields Equation 11.

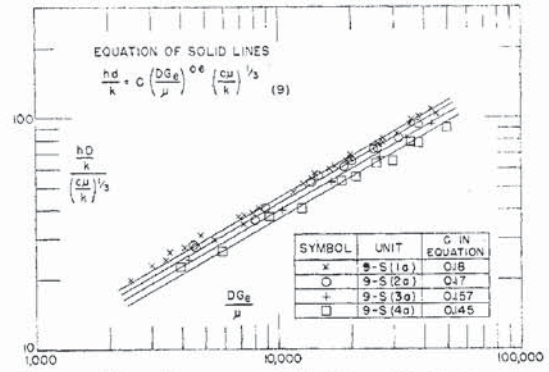

Figure 15. Segmental Baffles, Variation in Leakage Area

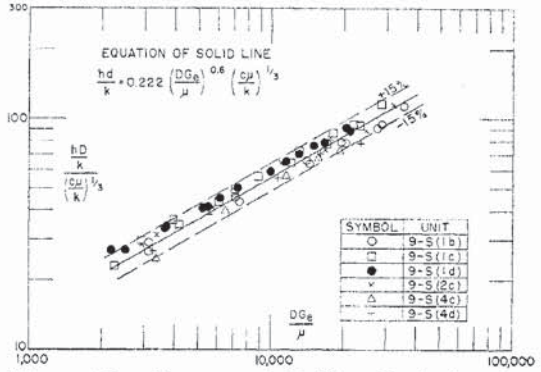

Figure 16. Segmental Baffles, Variation in Leakage Area

BAFFLES, BORED SHELLS

$$C\left(\frac{DG_e}{\mu}\right)^{0.6}\left(\frac{c\mu}{k}\right)^{0.33}\left(\frac{\mu}{\mu_w}\right)^{0.14}$$

Gardner and Siller				Tinker	Tinker	Tinker	Tinker	Tinker	Tinker	Tinker	Tinker	Tinker	Tinker
		G-S		1-T	2-T	3-T	4-T	5-T	6-T	7-T	8-T	9-T,10-T	11-T
		5.94		6.0	8.219	8.031	8.070	10.23	3.527	5.981	8.007	7.959	8.02
		3/8		3/8	3/8	3/8	3/8	3/8	3/8	3/8	5/8	3/8	5/8
		1/2		0.531	0.531	0.531	0.531	0.531	0.453	0.453	3/4	0.453	3/4
		80		92	170	170	170	262	40	124	68	243	68
		0.01		0.02	0.02	0.02	0.02	0.02	0.01	0.01	0.015	0.011	0.013
		0.03		0.094	0.25	0.062	0.101	0.07	0.017	0.023	0.067	0.037	0.044
		0.01892-0.0379		0.0417	0.0199	0.0186	0.0188	0.0382	0.00635	0.0188	0.0213	0.0507	0.043
		0.0563		0.041	0.043	0.04	0.041	0.0833	0.00653	0.0236	0.0362	0.047 and 0.095	0.0446
		0.668		0.57	0.61	0.57	0.57	0.63	0.37	0.37	0.74	0.3	0.74
Water	Velocite S	969 Oil	990 Oil	Water	Oil	Oil	Oil	Oil	Oil	Oil	Oil	Oil	Oil
0.432	6.3	16.8	55	0.432	25.2	25.2	25.2	25.2	25.2	25.2	25.2	25.2	25.2
		H & C		C	C	C	C	C	C	C	C	C	H & C
		17.2-14,900		2,360-10,400	84.3-537	12.4-523	4.33-303	26.8-182	10.7-199	16-554	215-556	208-990	4.19-2,060
		0.25		0.26	0.187	0.23	0.25	0.3	0.3	0.25	0.28	0.25	0.25
		75.8		78.7	56.7	69.7	75.8	91	91	75.8	84.9	75.8	75.8
		41		...	..	20	35.6	54.7	79.5	53	58.8	100	42.2
		63		67.1	38.8	55	63	81	86	63	76	63	63
		64		...	..	44.7	59.7	73.9	89.1	72.7	76.5	100	65
		0.985		...	..	1.23	1.05	1.10	0.97	0.866	0.993	0.63	0.97

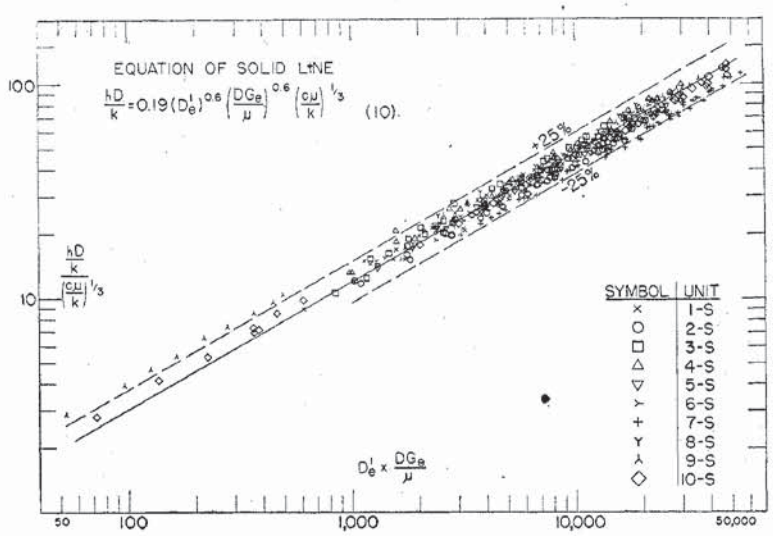

Figure 17. Heat Transfer Coefficient, Segmental Baffles

Short's experiments

$$\frac{hD}{k} = C\left(\frac{DG_e}{\mu}\right)^{0.6}\left(\frac{c\mu}{k}\right)^{0.33}\left(\frac{\mu}{\mu_w}\right)^{0.14} \qquad (11)$$

This was the same type of effect which had been noted for fluids inside tubes (*10*, *16*). The data of Gardner and Siller (*7*) are plotted in Figure 20 whose solid line has a value for C of 0.25 for Equation 11.

Summary and Discussion. For any given exchanger variations in baffle spacing and/or size of baffle cutout can be correlated by Equation 9. The effect produced by increasing leakage area has been noted to cause a decrease of approximately 20% in the coefficient of heat transfer. However, it should be noted that the clearances in experimental units 9-S(3a), 9-S(4a), 9-S(4c), 9-S(4d), and 2-T considerably exceeded industrial manufacturing tolerances and that leakage in these units was greater than would ordinarily be expected.

In a line of industrial heat exchangers of a certain style of construction—for example, the floating-head, removable tube-bundle-type shown in Figure 1—there will be considerable change in crossflow area and in baffle-cutout area over the entire range of sizes but these are taken care of by use of Equation 9. The effects produced by leakage areas and by tube arrangement which are expressed by the term C should remain relatively constant since the ratio of tube spacing to tube diameter is maintained constant, usually 1.25. Therefore, for industrial units, Equation 11A is proposed for unbored shells, and Equation 11B for bored shells.

DISK-AND-DOUGHNUT BAFFLES

The structural factors influencing G which have been studied are baffle spacing, size of baffle opening, and tube arrangement.

BAFFLE SPACING. The experimental test figures of Short (*14*) for unit 7-S are plotted in Figure 21 based on Equation 6 which employs G_c. (The crossflow area was taken as the minimum net free area based upon a circle equidistant from alternate baffle openings.) In exactly the same manner as was observed for segmental baffles, it was found that the heat transfer coefficient could not be correlated by use of a crossflow

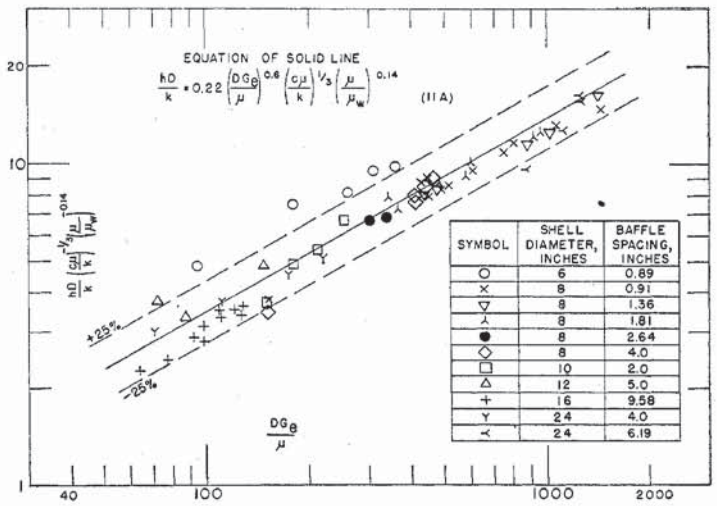

Figure 18. Segmental Baffles

Bowman's tests

TABLE V. COMPARISON OF CALCULATED AND OBSERVED VALUES OF h

(Variation in size of segmental baffle cutout)

Experimenter	Short	Short	Short	Short	Short	Short	Short	Short	Tinker	Tinker
Unit	9-S (1a)[a]	9-S (1b)	9-S (1c)	9-S (1d)	9-S (1a)[a]	9-S (1b)	9-S (1c)	9-S (1d)	9-T	10-T
Crossflow area, sq. ft.	0.0394	0.0394	0.0394	0.0394	0.0718	0.0718	0.0718	0.0718	0.0507	0.0507
Baffle cutout area, sq. ft.	0.01013	0.0207	0.0403	0.0726	0.01013	0.0207	0.0403	0.0726	0.047	0.095
S_e, sq. ft.	0.02	0.0286	0.0398	0.0535	0.0269	0.0386	0.0538	0.0724	0.0488	0.0694
Relative G_e	2.68	1.87	1.34	1	2.68	1.87	1.34	1	1.43	1
Relative $(G_e)^{0.6}$	1.81	1.46	1.2	1	1.81	1.46	1.2	1	1.23	1
Refer to Figure	12	12	12	12	13	13	13	13	14	14
Relative h from figure	1.35	1.27	1.2	1	1.38	1.25	1.15	1	1.18	1
Calcd. h/obsvd. h = relative $(G_e)^{0.6}$/relative h from figure	1.34	1.15	1	1	1.31	1.17	1.04	1	1.04	1

[a] Baffle cutout not long enough to direct flow across entire width of tube bundle.

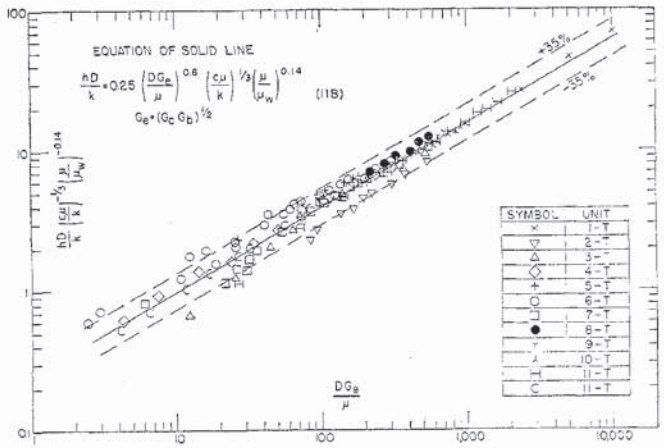

Figure 19. Segmental Baffles

Tinker's tests

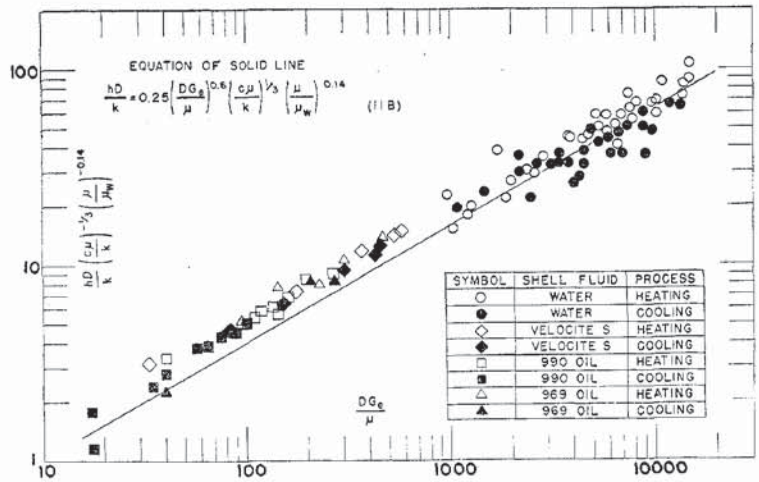

Figure 20. Heat Transfer Coefficient, Segmental Baffles

Gardner and Siller's tests

mass velocity or by a mass velocity at any other single section in the exchanger. In Figure 21 the value of C for 3 baffles is 2.1 times that for 19 baffles. Equation 9, which employs an averaged mass velocity based on the geometric mean of the velocities past the crossflow area and through the baffle opening, was used to correlate these same test points with the result shown in Figure 22.

SIZE OF BAFFLE OPENING. Examination of experimental test figures for segmental baffles revealed that baffle openings of widely different sizes can be correlated by using the geometric mean velocity of Equation 9. Short (*14*) in his experiments with disk-and-doughnut baffles ran tests on unit 5-S in which the only variable was the size of baffle opening; the other factors, such as tube size, tube pitch, number of tubes, baffle spacing, and tube-fluid velocity were constant. The results are shown in Figure 23 for the 19-, 11-, and 3-baffled units, respectively. The fluid flow, pounds per hour of water, is shown versus shell-side rate. Table VI lists for comparison the relative values of calculated and observed heat transfer coefficients in these units. The crossflow area has been assumed constant for all size openings leaving the weighted mass velocity, G_e, dependent solely upon the port velocity. Since coefficient of heat transfer is proportional to $(G_e)^{0.6}$, relative values will be the same as those shown in Table VI in the column headed relative $(G_e)^{0.6}$. These relative calculated values of heat transfer coefficient are seen to agree closely with the relative values obtained experimentally which are shown in the last column of Table VI.

TUBE ARRANGEMENT. The equation of the line of Figure 22 correlating the experimental test points for unit 7-S is

$$\frac{hD}{k} = 0.31 \left(\frac{DG_e}{\mu}\right)^{0.6} \left(\frac{c\mu}{k}\right)^{0.33} \qquad (9A)$$

C values for the other units were calculated and are listed in Table VII. These values were plotted on log-log paper and a straight line drawn through them which is described by the equation

$$C = 0.23(D_e')^{0.6} \qquad (4C)$$

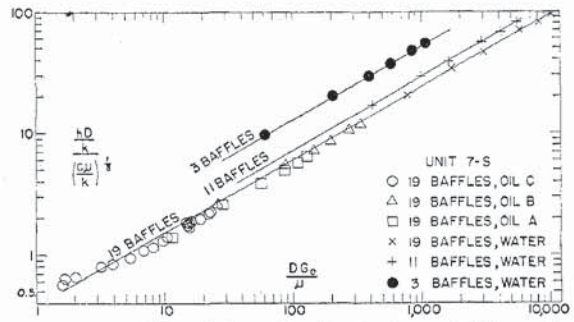

Figure 21. Heat Transfer Coefficient, Disk-and-Doughnut Baffles

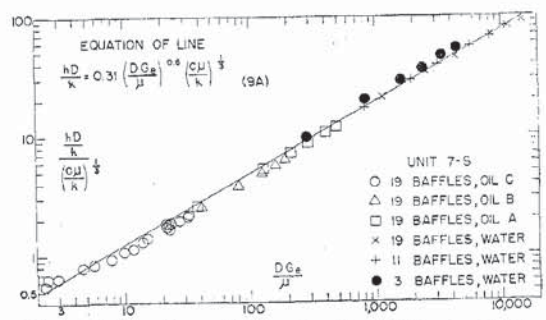

Figure 22. Heat Transfer Coefficient, Disk-and-Doughnut Baffles

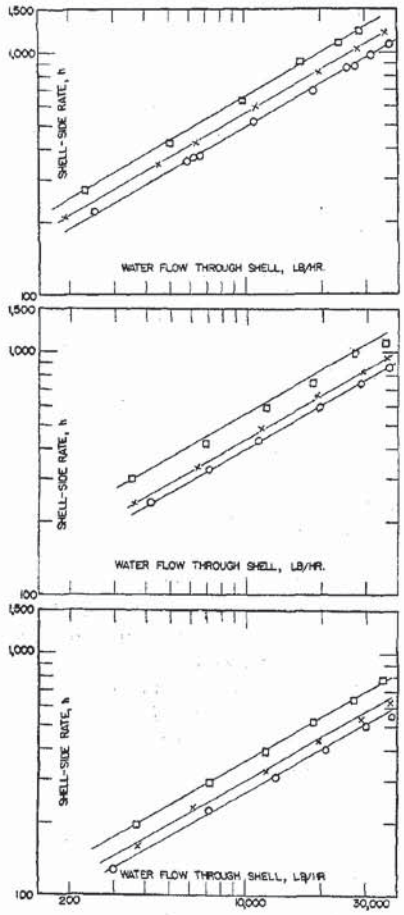

Figure 23. Effect of Size of Baffle Opening on Rate, Disk-and-Doughnut Baffles

(Above) ○ = 19 baffles, 4-inch hole, 5-S; × = 19 baffles, 3.5-inch hole, 5-S; □ = 19 baffles, 2.5-inch hole, 5-S
(Center) ○ = 11 baffles, 4-inch hole, 5-S; × = 11 baffles, 3.5-inch hole, 5-S; □ = 11 baffles, 2.5-inch hole, 5-S
(Below) ○ = 3 baffles, 4-inch hole, 5-S; × = 3 baffles, 3.5-inch hole, 5-S; □ = 3 baffles, 2.5-inch hole, 5-S

TABLE VI. COMPARISON OF CALCULATED AND OBSERVED VALUES OF h

(Variation in size of disk-and-doughnut baffle opening)

Number of Baffles	Hole Size, In.	Cross-flow Area, Sq. In.	Hole Area, Sq. In.	S_e, Sq. In.	Relative G_e	Relative $(G_e)^{0.6}$	Relative h from Figure
19	2.5	11.19	4.26	6.9	1.47	1.26	1.33, Figure 23 (top)
	3.5	11.19	7.46	9.15	1.11	1.06	1.13, Figure 23 (top)
	4	11.19	9.28	10.18	1	1	1, Figure 23 (top)
11	2.5	20.4	4.26	9.34	1.47	1.26	1.4, Figure 23 (center)
	3.5	20.4	7.46	12.35	1.11	1.06	1.1, Figure 23 (center)
	4	20.4	9.28	13.72	1	1	1, Figure 23 (center)
3	2.5	103	4.26	21	1.47	1.26	1.36, Figure 23 (bottom)
	3.5	103	7.46	27.7	1.11	1.06	1.13, Figure 23 (bottom)
	4	103	9.28	30.9	1	1	1, Figure 23 (bottom)

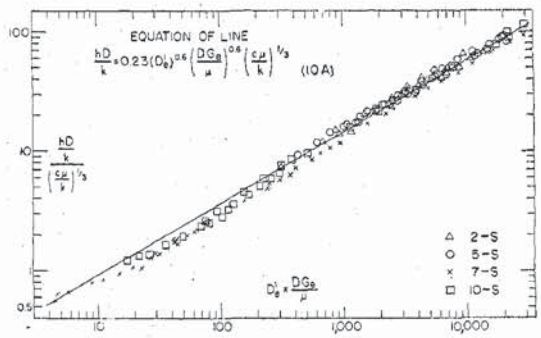

Figure 24. Heat Transfer Coefficient, Disk-and-Doughnut Baffles

The relationship already devised for correlating variations of baffle spacing and size of baffle opening in the same tube layout was Equation 9. Combination of Equations 9 and 4C yielded the general relationship for disk-and-doughnut baffles

$$\frac{hD}{k} = 0.23(D_e')^{0.6}\left(\frac{DG_e}{\mu}\right)^{0.6}\left(\frac{c\mu}{k}\right)^{0.33} \qquad (10A)$$

This equation was used to correlate all experimental test points of Short (*14*) in Figure 24 with an average deviation of ±11%.

PRESSURE DROP

The pressure drop on the shell side of a shell-and-tube exchanger is composed of losses resulting from: (*a*) enlargement and contraction in flowing through the nozzles, (*b*) flow parallel to the tubes, (*c*) flow through the baffle opening, and (*d*) flow across the tube bundle. Items *c* and *d*, of course, do not occur in unbaffled shells.

Unbaffled Shells. For the units studied the total pressure loss values were small and did not lend themselves to analysis because frictional losses could not be separated from nozzle losses. In comparison with those pressure losses which occur in baffled shells (the additional losses across the tube bundle, and through the baffle opening), pressure losses in unbaffled shells are negligible.

Segmental Baffles. PRESSURE DROP THROUGH BAFFLE OPENING. Using the experimental test figures of Short (*14*) it was found possible to isolate the first component of pressure drop, that resulting from flow through the baffle opening, by using those tests wherein baffle spacing was so great that the magnitude of pressure drop across the tube bundle was negligible compared to that through the baffle opening—namely, all tube layouts using three baffles. These data are shown in Figure 25 where mass velocity through the baffle opening is plotted versus pressure loss per baffle. Each unit tested had tubes passing through the baffle opening and the area for flow upon which G_b is based was taken as the area of the baffle cutout less the area of the tubes which passed through it. These areas are given on line 9 of Table II.

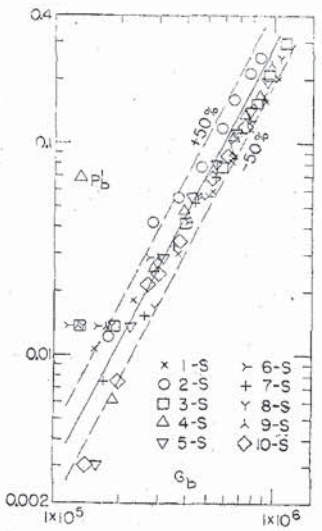

Figure 25. Pressure Loss through Opening in Segmental Baffle

In connection with the points of Figure 25 and other pressure-drop values, it may be noted that the values do not align themselves as closely to the straight-line relationship as do the values of heat transfer coefficient; they are more widely scattered, most points falling within ±50% of the straight-line relation of Figure 25 expressed by the equation

$$\Delta p_b' = \frac{2.9}{10^{13}}\frac{G_b^2}{\text{sp.gr.}} \qquad (12)$$

$$\Delta p_b' = 0.01392\ V^2\ \text{sp. gr.} \qquad (12A)$$

The average deviation of the points from the line is ±36%. Values of pressure drop exhibit wider fluctuations than do values of heat transfer coefficient because pressure drop is proportional to the square of the velocity whereas the heat transfer coefficient is proportional to the 0.6 power of the mass velocity. In connection with Figure 25 it should be pointed out that the tests were all run with water in turbulent flow; for streamline flow the friction factor was found to be higher than in turbulent flow with tests on orifice baffles.

TABLE VII. DISK-AND-DOUGHNUT BAFFLES, SHORT'S (*14*) TESTS

[Correlated by equation $\frac{hD}{k} = 0.23(D_e')^{0.6}\left(\frac{DG_e}{\mu}\right)^{0.6}\left(\frac{cp}{k}\right)^{0.33}$]

Unit	2-S	5-S	5-S	5-S	7-S	10-S
Shell, inside diameter, in.	6.06	6.06	6.06	6.06	6.06	6.06
Tube, outside diameter, in.	3/8	1/2	1/2	1/2	1/2	5/8
Tube pitch (equilateral triangle), in.	11/16	25/32	25/32	25/32	1 3/32	1 1/16
Number tubes	52	40	40	40	20	20
Diameter of baffle hole-tube diameter, in.	1/64	1/64	1/64	1/64	1/64	1/64
Inside shell diameter–baffle diameter, in.	Unbored shell	Unbored shell	Unbored shell	Unbored shell	Unbored shell	Unbored shell
Crossflow area, sq. ft.	0.1013–0.931	0.0776–0.715	0.0776–0.715	0.0766–0.715	0.1346–1.24	0.0992–0.91
Baffle cutout area, sq. ft.	0.0705	0.0296	0.0518	0.0643	0.0753	0.0676
Equivalent diameters of cross-sectional area, in.	1.12	1.0	1.0	1.0	1.94	1.52
Shell-side fluid	Water	Water	Water	Water	Water Oil A Oil B Oil C	Water Oil B
Viscosity at 150° F., centipoises	0.432	0.432	0.432	0.432	0.432 7.7 18.6 83	0.432 18.6
	C	C	C	C	C	C
Range of Reynolds number in Equation 9	77–10,280	193–15,130	140–13,700	365–16,500	70.8–10,400	3.12–15,900
Value of C in Equation 9	0.26	0.24	0.24	0.24	0.31	0.29

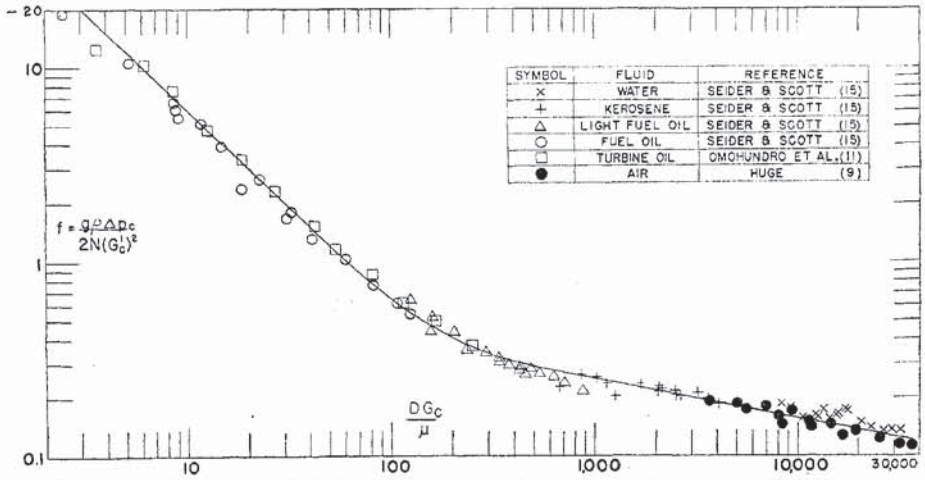

Figure 26. Isothermal Friction Factor, Flow across Staggered Tube Banks

***P/D* = 1.25**

The pressure drop of a fluid flowing through the segment cutout of a baffle may be considered as an orifice with a discharge coefficient of 0.7 (*5*). This may be transposed for comparison with Equation 12A as follows:

$$V = 0.7\sqrt{2gF} \tag{13}$$

$$\Delta p_b' = 0.00022\,\rho V^2 = 0.013\,72\,V^2\,\text{sp. gr.} \tag{13A}$$

Equations 12A and 13A show good agreement indicating that the segmental baffle behaves as an orifice with a discharge coefficient of 0.7. The circular holes in disk-and-doughnut baffles also conform to this same relation.

PRESSURE DROP ACROSS TUBE BUNDLE. After having isolated the effect of and developed an expression for pressure drop through the baffle opening as described above, the value so determined was subtracted from the over-all value of pressure drop and the difference was considered to be ascribable to frictional flow perpendicular to the tube bundle. The residual values of pressure drop so obtained were compared with those values which would be expected from the known relations for flow across tube banks.

The friction factor for flow across tube banks will be defined by the equation

$$f = \frac{g\rho\,\Delta p_c\Phi}{2N\,(G_e')^2} \tag{14}$$

throughout the entire range of Reynolds number. Tests of flow across tube banks have been reported by Sieder and Scott (*15*) who experimented with petroleum oils of a wide range of viscosity and with water, by Huge (*9*) and Pierson (*12*) who measured the pressure drop for air flow across tube banks which included a wide variety of tube spacings and arrangements, and by Omohundro, Bergelin, and Colburn (*11*) who carefully tested an oil in viscous flow. In Figure 26 their isothermal experimental data for tube arrangements in which tube spacing was 1.25 times tube diameter are plotted by use of Equation 14. The equation of the line for the viscous flow region is

$$f = \frac{60}{\frac{DG_e}{\mu}} \tag{15A}$$

and the equation of the line for turbulent flow is

$$f = \frac{0.99}{\left(\frac{DG_e}{\mu}\right)^{0.2}} \tag{16A}$$

These two straight lines merge gradually at the transition from viscous to turbulent region. For any ratio of tube spacing to tube diameter in the turbulent region Chilton and Genereaux (*2*) presented the general relation

$$f = \frac{0.75}{\left(\frac{P-D}{D}\right)^{0.2}\left(\frac{DG_e}{\mu}\right)^{0.2}} \tag{16}$$

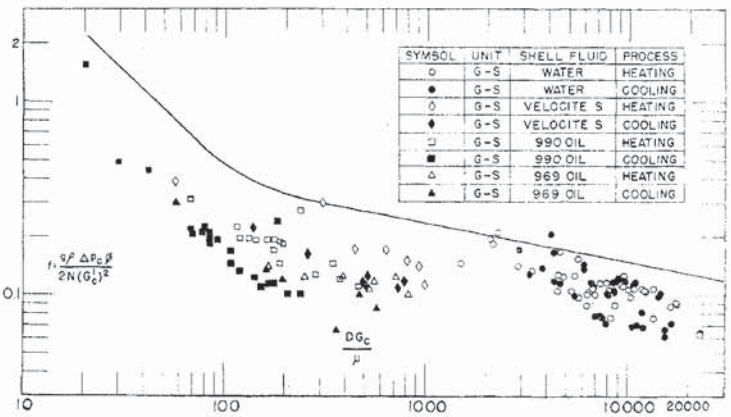

Figure 27. Friction Factor for Flow across Tube Bundle in Segmentally Baffled Units

***P/D* = 1.33**

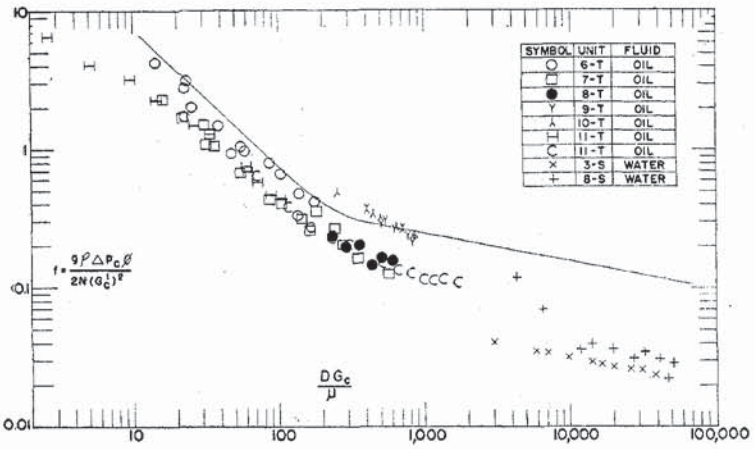

Figure 28. Friction Factor for Flow across Tube Bundle in Segmentally Baffled Units

***P/D* = 1.2**

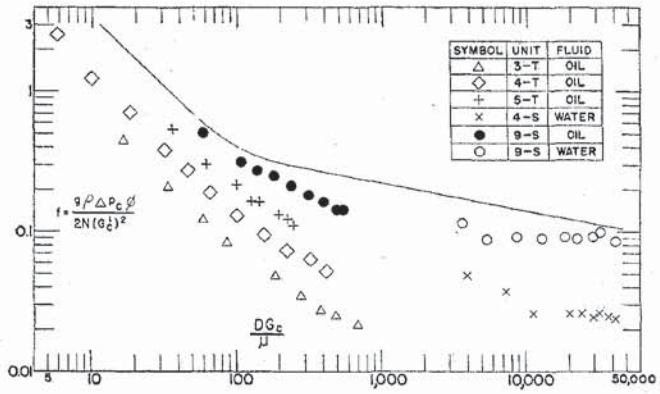

Figure 29. Friction Factor for Flow across Tube Bundle in Segmentally Baffled Units

***P/D* = 1.44**

In the region of viscous flow Sieder and Scott (*15*) tested a tube bank in which the P/D ratio was 1.582 and the equation was

$$f = \frac{26}{\frac{DG_c}{\mu}} \qquad (15B)$$

Following the method of Colburn (*3*) a general relation for other P/D ratios in the viscous region was estimated from Equations 15A and 15B to be

$$f = \frac{15}{\left(\frac{P-D}{D}\right)\left(\frac{DG_c}{\mu}\right)} \qquad (15)$$

Figures 27 to 29 show the experimental results obtained in many of the heat exchangers listed in Tables II and IV. In these Figures the solid lines represent the reference values of f for flow across a tube bank as obtained from Equations 15 and 16. The values of f obtained from experimental data have been calculated on the assumption that the entire quantity of flow penetrated the tube bank but it is evident, since most of the experimental values are below the reference line, that the flow did not completely penetrate the tube bank. In Figure 27 the P/D ratio is 1.33, in Figure 28 it is 1.2, and in Figure 29 it is 1.44.

Values of the ratio of the observed value of f as obtained from Equation 14 to the anticipated value of f for complete flow penetration as obtained from either Equations 15 or 16 are shown in Tables II and IV as effective % Δp_c. These values which are listed for Short's units in Table II are plotted against D_s' in Figure 30 and the equation of the line is

$$f \text{ (observed)}/f \text{ (calculated for full flow penetration} = 0.57\,(D_s')^2 \qquad (17)$$

This relation applies only to the units of Table II and does not apply to those of Table IV. Equations 12, 14, 16, and 17 were used to calculate values of pressure drop for the 413 tests run by Short (*14*) and the values so obtained were compared with observed values. The average deviation of calculated from observed values was approximately ±25%.

The available experimental data do not permit an evaluation of the numerical exponent to be used with (μ/μ_w) for the purpose of correlating heating and cooling operations. For want of more definite knowledge the exponent 0.14 has been used.

Disk-and-Doughnut Baffles. PRESSURE DROP THROUGH BAFFLE OPENING. The openings in disk-and-doughnut baffles, based on Short's (*14*) data, behave as orifices having a discharge coefficient of 0.7 and conform to Equation 12.

INTERDEPENDENCY OF COEFFICIENT OF HEAT TRANSFER AND FRICTION FACTOR

Wide variations in values of friction factor have been noted in Figures 27 to 29 and the variation has been ascribed to only part of the flow penetrating the tube bundle. The effects which fractional flow penetration will exert on friction factor and heat transfer coefficient may be readily computed when it is recalled that friction factor is a function of G^2 and heat transfer coefficient is a function of $G^{0.6}$. For example, if only half the total flow penetrates the tube bank the friction factor will be reduced to one quarter of the value for full penetration while the heat transfer coefficient will be reduced to two thirds the value for full penetration. The effect of varying amounts of flow penetration on coefficient of heat transfer and on friction factor is illustrated in Figure 31.

In order to apply this method of analysis to the heat exchangers on which tests had been reported it was necessary to set up reference relations, or optimum performance values, with which the observed values could be compared. For coefficient of heat transfer the relation of Colburn (*4*) for turbulent flow across tube banks

$$\frac{hD}{k} = 0.33\left(\frac{DG_c}{\mu}\right)^{0.6}\left(\frac{c\mu}{k}\right)^{0.33} \qquad (18)$$

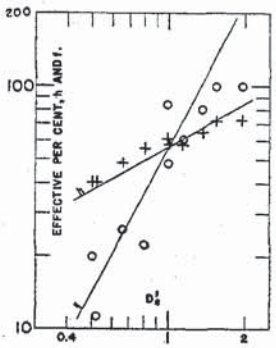

Figure 30. Relation of *h* and *f* to D_s' in Segmentally Baffled Units

+ = *h*, over-all heat transfer coefficient

○ = *f*, friction factor in crossflow

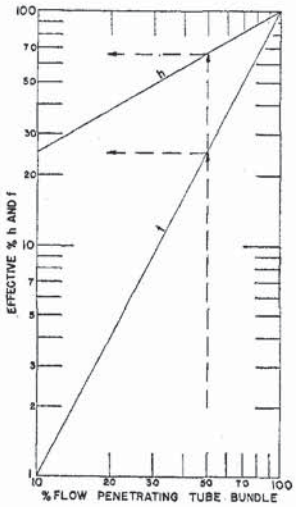

Figure 31. Effect of Flow Penetration on *h* and *f*

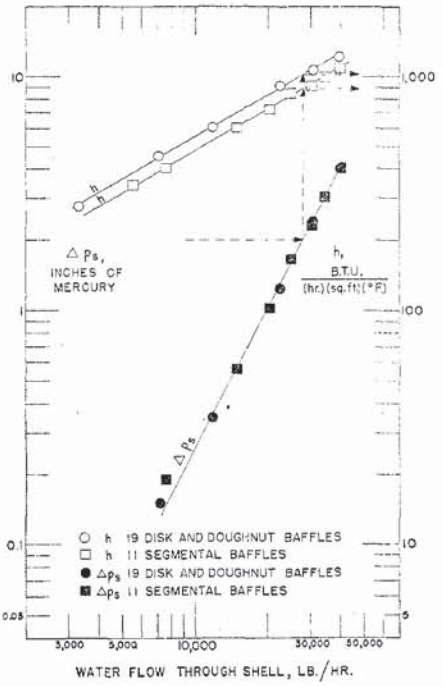

Figure 32. Comparison of Segmental with Disk-and-Doughnut Baffles, Unit 7-S

has been confirmed for a wide variety of tube arrangements by the experiments of Huge (*9*) and Pierson (*12*). If the value of G_b approximates that of G_c in a baffled exchanger the value of C in Equation 9 is here assumed to be 0.33 for full flow penetration. While there is evidence to indicate that the value of C is greater at small Reynolds numbers than the value of 0.33 which has been established for large Reynolds numbers, how much greater is not known, and for the present 0.33 will be used over the entire range of Reynolds number. The observed value of 100 (C/0.33) for an exchanger represents the effective per cent of coefficient of heat transfer and is listed in Tables II and IV. Equations 14 to 16 define the relations for friction factor for full flow penetration of the tube bundle. The ratio

$$100\left(\frac{f\text{ (observed)}}{f\text{(calculated for full flow penetration)}}\right)$$

represents the effective per cent of crossflow pressure drop and is shown in Tables II and IV.

The values from the last two lines of Table II have been plotted in Figure 30. The h line has a slope of 0.6 and the f line has a slope of 2 conforming to the pattern of Figure 31. Figure 31 has been employed to determine the per cent of flow penetration corresponding to the values of the effective per cents of coefficient of heat transfer and crossflow pressure drop of Table IV, and the values so determined are listed therein.

COMPARISON OF SEGMENTAL BAFFLES WITH DISK-AND-DOUGHNUT BAFFLES

It is interesting to compare disk-and-doughnut baffles with segmental baffles from the viewpoint of heat exchanger design for which the rate of fluid flow, pounds per hour, and the allowable pressure drop, pounds per square inch, are specified. These limitations govern the selection of size of the flow areas within the shell baffling. In Short's (*14*) exchanger, unit 7-S, it was found that when 19 disk-and-doughnut baffles were used the shell-side pressure drop was the same as when 11 segmental baffles were used, for a given rate of flow; however, the coefficient of heat transfer obtained with disk-and-doughnut baffles was approximately 15% greater than that obtained with segmental baffles. The experimental results are shown in Figure 32 where the rate of water flowing through the shell, pounds per hour, is plotted as abscissa and both heat-transfer coefficient h, and shell-side pressure drop Δp_s, are plotted as ordinates. Pressure-drop results for both units fall on a single line; coefficients of heat transfer fall on two separate lines, one for each unit. The broken lines show that for a flow of 28,000 pounds per hour of water the shell-side pressure drop in each unit is 2 inches of mercury and the coefficient of heat transfer for disk-and-doughnut baffles is 1,025 whereas for segmental baffles it is only 890. For all units tested, 2-S, 5-S, 7-S, and 10-S, disk-and-doughnut baffling showed higher coefficients of heat transfer than did segmental baffling; the magnitude of this superiority appeared to be 15% or better but was difficult to evaluate exactly because most test data did not permit direct comparison as was possible with unit 7-S, above.

The lower values for coefficient of heat transfer obtained with segmental baffling seem to indicate that some of the kinetic energy of the fluid is dissipated in eddy motion occurring in pockets in the flow path.

SUMMARY AND CONCLUSIONS

Heat transfer coefficients on the shell side of shell-and-tube exchangers conform to a relation of the form

$$\frac{hD}{k} = C\left(\frac{DG}{\mu}\right)^{0.6}\left(\frac{c\mu}{k}\right)^{0.33}\left(\frac{\mu}{\mu_w}\right)^{0.14} \qquad (1A)$$

In this equation values of C vary with the type of unit, and a mass velocity, G, having a rational basis is used to correlate the test data.

The published experimental data for unbaffled shells are correlated by the equation:

$$\frac{hD}{k} = 0.128(D_e')^{0.6}\left(\frac{DG_u}{\mu}\right)^{0.6}\left(\frac{c\mu}{k}\right)^{0.33} \qquad (5)$$

The coefficient of heat transfer for any baffled shell is expressed by the relation:

$$\frac{hD}{k} = C\left(\frac{DG_e}{\mu}\right)^{0.6}\left(\frac{c\mu}{k}\right)^{0.33}\left(\frac{\mu}{\mu_w}\right)^{0.14} \qquad (11)$$

in which G_e is the geometric mean of the mass velocities across the tube bundle and through the baffle opening.

The available experimental data for industrial heat exchangers having segmental baffles, reported by Bowman (*1*) and Tinker (*17*), indicate approximate C values in Equation 11 of 0.22 for unbored shells and 0.25 for bored shells. Dimensions of these units are listed in Tables III and IV.

The pressure loss of flow through baffle openings is defined by Equation 12 which is the same as for an orifice with a discharge coefficient of 0.7.

Experimental pressure-drop values exhibit considerable variation for small differences in shell-side structure showing different fractions of total flow penetrating the tube bundle. The effect of partial flow penetration on h and f is shown in Figure 31.

Interdependency of h and f is shown in Figure 30 and in Tables II and IV.

Disk-and-doughnut baffles produced higher coefficients of heat transfer than did segmental baffles, at equal values of fluid flow rate and pressure drop, in all units tested. This difference may result from eddy motion energy losses occurring in dead pockets in the flow path through segmental baffling.

ACKNOWLEDGMENT

The author is grateful to Thomas F. Gould for assistance in reviewing the manuscript, and to Byron E. Short for his cooperation in furnishing data.

NOMENCLATURE

$B.P.$ = baffle spacing, inches
c = specific heat, B.t.u./(lb.)(° F.)
C = numerical values in heat transfer equation
D = outside tube diameter, ft.
D_e = equivalent diameter = 4 × (flow area/wetted perimeter), ft.
D_e' = equivalent diameter = 4 × (flow area/wetted perimeter), inches
D_i = inside tube diameter, ft.
f = friction factor
f (calculated for full flow penetration) = friction factor defined by Equations 15 and 16 in which G equals total flow divided by crossflow area

f (observed) = friction factor calculated from Equation 14 in which G_s' equals total flow divided by crossflow area, and $\Delta p_c'$ is the observed value of crossflow pressure drop
F = height of fluid head, ft.
g = gravitational constant, 32.17 ft./(sec.)(sec.).
G = mass velocity, lb./(hr.)(sq.ft).
G_b = mass velocity through baffle opening, based upon the area of the opening less the area of the tubes passing through it, lb./(hr.)(sq.ft).
G_c = crossflow mass velocity, lb./(hr.)(sq.ft.)
G_s' = crossflow mass velocity, lb./(sec.)(sq.ft.)
G_e = weighted mass velocity = w/S_e = $(G_c G_b)^{0.5}$, lb./(hr.)(sq.ft.)
G_t = mass velocity inside tubes, lb./(hr.)(sq.ft).
G_u = mass velocity parallel to tubes = total flow/(cross-sectional area of shell − cross-sectional area of tubes), lb./(hr.)(sq.ft.)
h = coefficient of heat transfer, B.t.u./(hr.)(sq.ft)(° F.)
k = thermal conductivity, B.t.u./(hr.)(sq.ft.)(° F.)/(ft.)
N = number of rows of tubes crossed
P = tube spacing, center to center, ft.
$P - D$ = clearance between tubes, ft.
S_e = weighted flow area = $\sqrt{\text{crossflow area} \times \text{baffle-hole area}}$, sq. ft.
sp.gr. = specific gravity referred to water at 60° F.
V = linear velocity, ft./sec.
w = rate of flow, lb./hr.
$\Delta p_b'$ = pressure drop through baffle opening, per baffle, lb./sq. in.
Δp_c = pressure drop across tube bundle, lb./sq.ft.
Δp_s = total shell-side pressure drop, inches of mercury
μ = viscosity at average temperature, lb./(hr.)(ft.)
μ_w = viscosity at tube wall temperature, lb./(hr.)(ft.)
ρ = density, lb./cu.ft.
Φ = viscosity-gradient factor, $\left(\frac{\mu}{\mu_w}\right)^{0.14}$

LITERATURE CITED

(1) Bowman, R. A., *Am. Soc. Mech. Engrs., Miscellaneous Papers*, No. 28, 75–81 (1936).
(2) Chilton, T. H., and Genereaux, R. P., *Trans. Am. Inst. Chem. Engrs.*, 29, 161–73 (1933).
(3) Colburn, A. P., *Purdue Univ. Eng. Bull.* No. 84 (Vol. 26, No. 1), 37 (1942).
(4) Colburn, A. P., *Trans. Am. Inst. Chem. Engrs.*, 29, 174–210 (1933).
(5) Drew, T. B., and Genereaux, R. P., "Chemical Engineers' Handbook," Perry, J. N., ed., 2nd ed., 828–9, New York, McGraw-Hill Book Co., 1941.
(6) Gardner, H. S., and Siller, Irving, *Trans. Am. Soc. Mech. Engrs.*, 69, 687–94 (1947).
(7) Gardner, H. S., and Siller, Irving, unpublished tabulation of the experimental data of reference (*6*).
(8) Heinrich, E., and Stückle, R., *Ver. deut. Ing., Mitt. Forsch. Gebiete Ingenieurw., Heft* 271 (1925).
(9) Huge, E. C., *Trans. Am. Soc. Mech. Engrs.*, 59, 573–81 (1937).
(10) Keevil, C. S., and McAdams, W. H., *Chem. & Met. Eng.*, 36, 464–7 (1929).
(11) Omohundro, G. A., Bergelin, O. P., and Colburn, A. P., *Trans. Am. Soc. Mech. Engrs.*, 71, 27–34 (1949).
(12) Pierson, O. L., *Ibid.*, 59, 563–72 (1937).
(13) Short, B. E., paper presented at the Am. Soc. Mech. Engrs.' Annual Meeting, Atlantic City, N. J., Dec. 1 to 5, 1947.
(14) Short, B. E., *Univ. Texas Pub.* No. 4324, 1–55 (1943).
(15) Sieder, E. N., and Scott, N. A., Jr., *Am. Soc. Mech. Engrs., Unpublished Papers*, No. 83 (1932).
(16) Sieder, E. N., and Tate, G. E., IND. ENG. CHEM., 28, 1429–35 (1936).
(17) Tinker, Townsend, paper presented at the Am. Soc. Mech. Engrs.' Annual Meeting, Atlantic City, N. J., Dec. 1 to 5, 1947.
(18) Wilson, E. E., *Trans. Am. Soc. Mech. Engrs.*, 37, 47 (1915).

RECEIVED November 5, 1947.

Synthetic Gasoline from Natural Gas

COMPOSITION AND QUALITY

F. H. BRUNER

The Texas Company, Beacon, N. Y.

Gasoline produced in this country by the fluidized iron-catalyzed hydrogenation of carbon monoxide is of much higher quality than that produced commercially in Europe by the Fischer-Tropsch fixed-bed, cobalt-catalyzed process. In contrast to the high boiling, paraffinic material produced over cobalt, the hydrocarbons produced by the American process are relatively low boiling and highly olefinic. The olefins are characterized as straight chain or monomethyl with the double bond in the 1-position. This permits the conversion of the gasoline to a high octane fuel or blending stock by a simple catalytic treatment. A 7-pound Reid vapor pressure, 400° F. end point naphtha has an A.S.T.M. D-357 motor octane of 82 and an A.S.T.M. D-908 research octane. The synthetic fuel blends normally in straight-run and cracked products.

MUCH publicity has been given lately to the American synthetic gasoline process known as the Hydrocol process which has reached the commercialization stage for the production of gasoline from natural gas. Most of the information thus far published has dealt with the process side of the synthesis and has given only general information as to the composition and quality of the resulting synthetic fuel. The purpose of this paper is to present information on the hydrocarbon distribution in the gasoline fraction and to describe briefly its further processing to produce a satisfactory component for present-day motor fuels.

"Synthetic gasoline from natural gas" can have a number of meanings, since there are a variety of ways of converting the hydrocarbons in natural gas into higher boiling material which might fall under the broad classification of synthetic gasoline. The term, however, as used here, is the more popular usage which refers to the product from the catalytic hydrogenation of carbon monoxide; this is by far the most practical definition. The hydrogen and carbon monoxide in turn are produced by the non-catalytic combustion of natural gas in substantially pure oxygen. This reaction results in the production of a carbon monoxide–hydrogen mixture of relatively high purity having an approximate ratio of 2 volumes of hydrogen to 1 volume of carbon monoxide. The specific gasoline discussed here was obtained in Texas Company pilot units in a manner similar to that which will be employed in commercial Hydrocol units.

However, as a 2 to 1 hydrogen to carbon monoxide mixture is not unique to the combustion of natural gas and as the source of the carbon monoxide and the hydrogen is not evident in the re-